electronics

MDPI

Article

Adaptive Learning from Quantized Signals for AUV Formation Tracking Control

Chao Wang [1], Xiaolei Li [2,*], Pengfei Yang [2], Jiange Wang [2] and Yuzhong Wang [3]

[1] Beijing Zhongqi Anhuan Information Science Research Institute, Beijing 100089, China
[2] School of Electrical Engineering, Yanshan University, Qinhuangdao 066004, China
[3] Department of Mechanical Engineering, The University of Hong Kong, Hong Kong
* Correspondence: xiaolei@ysu.edu.cn

Abstract

This paper investigates the formation tracking problem for a group of autonomous underwater vehicles (AUVs) operating under quantized communication and actuation. A novel adaptive learning framework is proposed, capable of extracting cooperative control policies directly from quantized relative measurements and quantized input signals. Unlike conventional approaches that rely on continuous signal assumptions, the developed method enables each AUV to learn and adapt its behavior in real time from coarsely quantized data, thereby enhancing robustness in digital and bandwidth-limited environments. Within a backstepping control structure, an improved quantized consensus mechanism and a hysteresis quantizer compensation strategy are integrated to mitigate quantization effects. Using Lyapunov stability theory, it is proven that all closed-loop signals remain bounded and the formation tracking errors converge to an adjustable neighborhood of zero. Simulation results demonstrate that the proposed learning-based controller achieves accurate formation tracking and exhibits strong adaptability under dual quantization constraints.

Keywords: AUVs; coordination control; adaptive tracking; quantized measurement; quantized input

1. Introduction

The ability of autonomous underwater vehicles (AUVs) to operate independently in submerged environments presents prospective benefits for carrying out tasks related to monitoring marine pollution, hydrological features, and marine ecosystems [1–5]. Collaborative tracking control of AUVs is a complex technology involving multiple AUVs working together to perform tasks together. Multi-AUVs can improve mission efficiency while coping with more complex underwater environments, providing new possibilities for marine research, resource exploration, etc. [6,7]. Therefore, the collaborative tracking control of AUVs has captured the attention of researchers, but it also faces many difficulties in control design. Solving these challenges will not only promote the further development of multi-AUV technology but also broaden underwater scientific research and industrial application possibilities.

1.1. Related Works

The development of coordinated controllers for AUVs is critical for achieving fast, accurate, and stable system performance. Several advanced algorithms and strategies have been proposed to enhance the control capabilities of AUVs. For instance, ref. [8]

Academic Editor: Ahmed Abu-Siada

Received: 1 April 2026
Revised: 27 April 2026
Accepted: 4 May 2026
Published: 11 May 2026

 https://doi.org/10.3390/electronics15102050

introduced a distributed bionic sliding mode controller for multi-AUV systems, which effectively mitigated the jitter issues inherent in traditional sliding mode control (SMC). However, this approach remains vulnerable to noise interference. Leveraging the redistribution mechanism of leader–follower formation, ref. [9] proposed a novel formation strategy for nonlinear uncertain systems. While this method demonstrated excellent formation convergence, it also introduced higher computational complexity. To address this, ref. [10] developed a distributed nonlinear model predictive control (NMPC) algorithm that reduces computational demands by exploiting the dynamic characteristics of AUV motion. Additionally, ref. [11] presented a coordinated tracking strategy tailored for multiple AUVs operating in complex ocean environments. Despite these advancements, the majority of these methods focus on simplified two-dimensional scenarios and rely on reduced-order dynamic models for controller design.

Several advanced control frameworks have been developed for uncertain nonlinear systems, among which state-filtered disturbance rejection methods and neuroadaptive reinforcement learning approaches are particularly representative. Disturbance rejection techniques, such as extended state observers (ESOs), uncertainty and disturbance estimators (UDEs), and active disturbance rejection control (ADRC), estimate lumped uncertainties and compensate them online, thereby achieving strong robustness against modeling errors and external disturbances. However, these methods usually rely on continuous and sufficiently accurate state measurements. When only quantized relative measurements and quantized actuator inputs are available, observer performance may deteriorate significantly, and quantization effects are often treated merely as external disturbances, resulting in conservative designs. On the other hand, multilayer neural network and actor–critic reinforcement learning methods have demonstrated strong approximation and optimization capabilities for nonlinear control problems. Nevertheless, most of these approaches require high-quality state information, informative reward signals, and repeated online exploration, while their computational complexity may be prohibitive for embedded AUV platforms with limited onboard resources. In addition, the interplay between distributed cooperation and dual quantization constraints is rarely addressed explicitly. Motivated by these limitations, this paper develops a lightweight adaptive learning framework for multi-AUV formation tracking under quantized communication and quantized actuation. Different from existing observer-based or neural approximation methods, the proposed controller directly synthesizes cooperative policies from quantized relative measurements through a distributed consensus mechanism integrated with backstepping design. Meanwhile, a hysteresis-quantizer compensation strategy is constructed according to explicit quantization error bounds, and the closed-loop stability is rigorously established via Lyapunov analysis. Therefore, the proposed method is particularly suitable for bandwidth-limited and digitally implemented underwater cooperative systems.

In recent years, considerable attention has been devoted to the stability analysis and control design of systems subject to quantized signals. Quantization is unavoidable in practical digital control systems and bandwidth-limited communication environments. In [12,13], direct adaptive control frameworks were proposed for linear and nonlinear uncertain systems with input quantizers, and Lyapunov-based stability analysis was provided. The work in [14] investigated event-triggered control of nonlinear systems under state quantization, where communication usage was reduced by the event-triggered mechanism. In [15], a neural-network-based adaptive control method was developed for nonlinear systems with quantized inputs and output constraints. Furthermore, ref. [16] studied adaptive output-feedback control for nonlinear systems with input/output quantization and mismatched uncertainties. Although these studies provide important theoretical foundations for quantized control, most of them focus on single-agent nonlinear systems or general uncertain systems. The distributed formation tracking problem of multiple AUVs under simultaneous quantized relative measurements and quantized actuator inputs remains insufficiently addressed.

1.2. Contributions

Inspired by above discussions, this paper considers the cooperative tracking control problem of a group for AUVs with quantized measurements and input signals. The backstepping method is used to design the quantized cooperative controller and Lyapunov function is used to analyze the performance and stability of the closed-loop system. The main contributions of this paper are summarized as follows.

1. An adaptive learning framework is proposed for AUV formation control, which enables each vehicle to synthesize cooperative control policies directly from quantized relative measurements and quantized actuator inputs, eliminating the reliance on continuous signal assumptions and better aligning with digital implementation realities.
2. An improved quantized consensus algorithm is developed within the learning-based structure, which facilitates distributed coordination under coarse measurement quantization, enhancing the scalability and robustness of multi-AUV systems in bandwidth-limited environments.
3. A compensation strategy with a hysteresis quantizer is integrated into the learning-based controller to mitigate the effects of input quantization. By appropriate parameter selection, the quantization-induced errors are confined to an arbitrarily small region, ensuring stable formation tracking performance.

The paper is structured as follows: In Section 2, the AUV's kinematic and dynamic models, as well as the control objectives and some preliminaries, are presented. In Section 3, an adaptive controller is designed using the back-stepping method, and the stability and performance of the closed-loop system are examined by presetting the relevant Lyapunov functions. The simulation results are given in Section 4 to demonstrate the effectiveness of the proposed control algorithm. In Section 5, the entire work is summed up, which also suggests potential future research areas.

2. Problem Formulation

In this section, the kinematic and dynamic models of the AUV are presented. Furthermore, the control objectives of this paper are proposed. Then, the relevant background knowledge of graph theory and the mathematical formulas of the two quantizers used in this paper are given.

2.1. Kinematics and Dynamics Model of AUV

The considered AUV system is shown in Figure 1. The position of AUV i are expressed in an earth-fixed frame, which is described as $\boldsymbol{\eta_{1i}} = [x_i, y_i, z_i]^\top \in \mathbb{R}^3$. The orientation is denoted by $\boldsymbol{\eta_{2i}} = [\phi_i, \theta_i, \psi_i]^\top \in \mathbb{R}^3$ in the earth-fixed frame, which can be represented by a rotation matrix $\boldsymbol{R}_{Ii}^B$. The rotation matrix $\boldsymbol{R}_{Ii}^B$ represents the transformation from the earth-fixed frame to the vehicle-fixed frame. The superscript indicates the reference frame to which the vector points. We define $\boldsymbol{\eta_i} = [\boldsymbol{\eta}_{1i}^\top, \boldsymbol{\eta}_{2i}^\top]^\top$, the time derivatives that correspond to it are expressed as $\dot{\boldsymbol{\eta}}_i = [\dot{\boldsymbol{\eta}}_{1i}^\top, \dot{\boldsymbol{\eta}}_{2i}^\top]^\top$. The linear and angular velocities of AUV i are defined in the vehicle-fixed frame, and their expressions are $\boldsymbol{\nu}_{1i} = [u_i, v_i, w_i]^\top \in \mathbb{R}^3$ and $\boldsymbol{\nu}_{2i} = [p_i, q_i, r_i]^\top \in \mathbb{R}^3$; then, we define $\boldsymbol{\nu}_i = [\boldsymbol{\nu}_{1i}^\top, \boldsymbol{\nu}_{2i}^\top]^\top$.

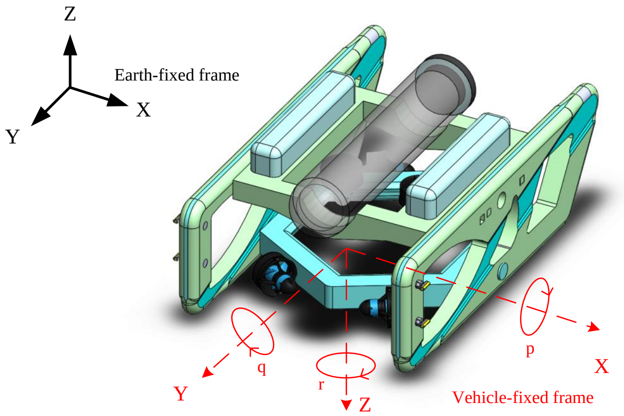

Figure 1. Schematic diagram of an AUV.

The relationship between velocity $\boldsymbol{\nu}_i$ and the derivative of position and attitude $\dot{\boldsymbol{\eta}}_i$ can be expressed as

$$\boldsymbol{\nu}_i = \begin{bmatrix} \boldsymbol{R}_{Ii}^{B} & \boldsymbol{O}_{3\times3} \\ \boldsymbol{O}_{3\times3} & \boldsymbol{T}(\eta_{2i}) \end{bmatrix} \begin{bmatrix} \dot{\boldsymbol{\eta}}_{1i} \\ \dot{\boldsymbol{\eta}}_{2i} \end{bmatrix}, \tag{1}$$

where

$$\boldsymbol{T}(\boldsymbol{\eta}_{2i}) = \begin{bmatrix} 1 & 0 & -s_{\theta i} \\ 0 & c_{\phi i} & c_{\theta i}s_{\phi i} \\ 0 & -s_{\phi i} & c_{\theta i}c_{\phi i} \end{bmatrix}. \tag{2}$$

where s_a and c_a are the abbreviation of $sin(a)$ and $cos(a)$, respectively.

From [17], the dynamics model of the ith AUV with control input quantization can be expressed as

$$\boldsymbol{M}_i\dot{\boldsymbol{\nu}}_i + \boldsymbol{C}_i(\boldsymbol{\nu}_i)\boldsymbol{\nu}_i + \boldsymbol{D}_i(\boldsymbol{\nu}_i)\boldsymbol{\nu}_i + \boldsymbol{g}_i = q(\boldsymbol{\tau}_i)\ \ , \tag{3}$$

where $\boldsymbol{M}_i$ is the inertia matrix of AUV i, $\boldsymbol{C}_i(\boldsymbol{\nu})$ and $\boldsymbol{D}_i(\boldsymbol{\nu})$ are the vectors of Coriolis and centripetal terms and friction and hydrodynamic damping terms, $\boldsymbol{g}_i$ is the vectors of gravitational and buoyant generalized forces, and $\boldsymbol{\tau}_i$ is the forces and moments of the vehicle. $q(\boldsymbol{\tau}_i)$ represents the hysteretic quantizer and takes the quantized values. More details for the kinematics model of AUV can be seen in [17].

Note that the following properties are well known for Equation (3), the details can be seen in [18].

P1: The inertia matrix $\boldsymbol{M}_i$ is positive definite and symmetric.

P2: The matrix $\boldsymbol{M}_i - 2\boldsymbol{C}_i(\boldsymbol{\nu}_i)$ is skew symmetric, i.e., $x^{\mathrm{T}}(\boldsymbol{M}_i - 2\boldsymbol{C}_i(\boldsymbol{\nu}_i))x = 0$ for any nonzero vector $x \in \mathbb{R}^6$.

P3: The damping matrix $\boldsymbol{D}_i(\boldsymbol{\nu}_i)$ is positive definite.

2.2. Control Objective

The objective of this paper is to control a group of AUVs to converge and remain in a preset polygon so that the circumcenter of the polygon can move along the desired trajectory. Every AUV is capable of achieving the required attitude in accordance with mission requirements when it comes to attitude control. We let the desired trajectory be $\boldsymbol{\eta}_{1d} = [x_d, y_d, z_d]^{\mathrm{T}}$, and the desired attitudes of this group of AUVs are $\boldsymbol{\eta}_{2id} = [\phi_{di}, \theta_{di}, \psi_{di}]^{\mathrm{T}}, i = 1, \ldots, n$, which is supposed to be an arbitrarily smooth curve. Given a desired geometric pattern formed by n vertices, the offsets of each vertex relative to the circumcenter of the desired geometric pattern are defined as $\boldsymbol{d}_i = [d_{xi}, d_{yi}, d_{zi}]^{\mathrm{T}}$.

The control problem boils down to designing a collaborative controller based on each AUV local state, relative measurements, and the position of the circumcenter such that the following results can be achieved:

$$\lim_{t\to\infty}\left\|\begin{bmatrix} x_i - x_j \\ y_i - y_j \\ z_i - z_j \end{bmatrix} - \begin{bmatrix} d_{xi} - d_{xj} \\ d_{yi} - d_{yj} \\ d_{zi} - d_{zj} \end{bmatrix}\right\| < \delta, \tag{4}$$

and

$$\lim_{t\to\infty}\left\|\begin{bmatrix} \frac{1}{n}\sum_{i=1}^{n} x_i \\ \frac{1}{n}\sum_{i=1}^{n} y_i \\ \frac{1}{n}\sum_{i=1}^{n} z_i \end{bmatrix} - \begin{bmatrix} x_{ed} \\ y_{ed} \\ z_{ed} \end{bmatrix}\right\| < \delta. \tag{5}$$

where $\delta > 0$ is a small scalar, which gives it later. Equation (4) proves the rationality of cooperative control, which means that a group of AUVs can converge and maintain the preset geometry. Equation (5) verifies that the circumcenter of the preset polygon can converge to the desired trajectory.

Remark 1. *Here, $\boldsymbol{d}_i$ is a constant, so the preset graph is unchanged. In order to overcome this limitation and improve the flexibility of cooperative control, we can consider $\boldsymbol{d}_i$ as time-varying offsets to update the preset graph composed of the group of AUVs.*

Furthermore, each AUV completes desire attitude tracking, which is defined as

$$\lim_{t\to\infty}\|\boldsymbol{\eta}_{2i} - \boldsymbol{\eta}_{2id}\| < \delta. \tag{6}$$

2.3. Graph Theory

Graph theory is often used to describe the specific relationships between certain entities and is an excellent tool for describing communication relationships between AUVs. We let $\boldsymbol{G} = (\boldsymbol{V}, \boldsymbol{E}, \bar{\boldsymbol{A}})$ denote the communication topology between the n AUVs. Here, $\boldsymbol{V}$ is a set of nodes, $\boldsymbol{E} \subseteq \boldsymbol{V} \times \boldsymbol{V}$ represents the set of edges, $\bar{\boldsymbol{A}} = [a_{ij}] \in \boldsymbol{R}^{n\times n}$, $a_{ij} \geq 0$ represents a adjoint matrix of the topological graph G. The Laplacian matrix of a weighted graph $\boldsymbol{G}$ is $\boldsymbol{L} = \boldsymbol{\mathcal{D}} - \bar{\boldsymbol{A}}$, where $\boldsymbol{\mathcal{D}} = \mathrm{diag}\{d_1, \cdots, d_n\}$, $d_i = \sum_{j=1}^{n} a_{ij}$. For undirected graphs, the transmission of information is bidirectional, that is, $a_{ij} = a_{ji}$. We suppose that the underlying communication topology is connected. Thus, the Laplacian matrix of a weighted graph $\boldsymbol{G}$ can be decomposed into $\boldsymbol{L} = D^{\top} D$ with $D \in R^{n\times n-1}$ is a full rank incidence matrix.

Remark 2. *In this paper, the communication topology is assumed to be connected and time-invariant for analytical clarity. This assumption is commonly adopted as a first-step framework in distributed cooperative control and allows the main focus to be placed on the simultaneous effects of quantized relative measurements and quantized actuator inputs. It is worth noting that the proposed control strategy only relies on local neighbor information exchange and can be naturally extended to time-varying or switching communication graphs by replacing the constant Laplacian matrix $\mathbf{L}$ with a time-dependent Laplacian $\mathbf{L}(t)$. If the switching topology satisfies a joint-connectivity condition, i.e., the union of the communication graphs over each bounded time interval contains a spanning tree or remains connected, then the cooperative tracking mechanism can still preserve consensus and formation convergence properties. For intermittent communication caused by packet dropouts or temporary acoustic channel blockage, temporary disconnections mainly affect the transient convergence rate and may enlarge the short-term tracking error. Nevertheless, the local stabilizing feedback terms and quantization–compensation mechanism still help maintain bounded closed-loop signals. A rigorous extension of the present results to switching and intermittent topologies requires* *hybrid-system analysis tools, such as common Lyapunov functions or multiple Lyapunov function techniques, and will be investigated in our future work.*

2.4. Quantizer

In this paper, the quantized relative measurement and input signals are considered in control design of the AUVs. In this context, the logarithm quantizer is considered, which is introduced as

$$Q(u) = \begin{cases} u_j \operatorname{sign}(u), & \frac{u_j}{1+\sigma} \leq |u| \leq \frac{u_j}{1-\sigma} \\ 0, & |u| < \frac{u_0}{1+\sigma} \end{cases} \tag{7}$$

where $u_j = \rho_1^{(1-i)} u_0$, $i = 1, 2, \ldots, \rho_1 \in (0, 1)$, $\rho_1 = \frac{1-\sigma}{1+\sigma}$, $0 < \sigma < 1$. u_0 is the quantization dead zone and ρ_1 is the quantized density. The logarithmic quantizer satisfies

$$|Q(u) - u| \leq \frac{\sigma}{2}. \tag{8}$$

For the control signal, a hysteretic quantizer [19] is considered, which is represented as

$$q(u(t)) = \begin{cases} u_i \operatorname{sgn}(u), & \frac{u_i}{1+\delta} < |u| \leq u_i, \dot{u} < 0, \text{ or} \\ & u_i < |u| \leq \frac{u_i}{1-\delta}, \dot{u} > 0 \\ u_i(1+\delta) \operatorname{sgn}(u), & u_i < |u| \leq \frac{u_i}{1-\delta}, \dot{u} < 0, \text{ or} \\ & \frac{u_i}{1-\delta} < |u| \leq \frac{u_i(1+\delta)}{(1-\delta)}, \dot{u} > 0 \\ 0, & 0 \leq |u| < \frac{u_{\min}}{1+\delta}, \dot{u} < 0 \text{ or} \\ & \frac{u_{\min}}{1+\delta} \leq u \leq u_{\min}, \dot{u} > 0, \\ q(u(t^-)) & \dot{u} = 0 \end{cases} \tag{9}$$

where $u_i = \rho_2^{(1-i)} u_{\min}$, $i = 1, 2, \ldots, \rho_2 \in (0, 1)$, $\rho_2 = \frac{1-\delta}{1+\delta}$, $0 < \delta < 1$. $u_{\min}$ is the quantization dead zone and ρ_2 is the quantized density. Then, the following lemma is presented:

Lemma 1. *We define $q(u) = u + \mu$ with μ bing the hysteresis quantizer error, then the quantizer error satisfies the following inequalities:*

$$\mu^2(t) \leq \delta^2 u^2, \forall |u| \geq u_{\min}. \tag{10}$$

$$\mu^2(t) \leq u_{\min}^2, \forall |u| \leq u_{\min}. \tag{11}$$

Proof. As shown in Figure 2, for the case that $u \geq u_{\min}$, it yields

$$(1-\delta)u \leq q(u) \leq (1+\delta)u,$$

which leads to

$$|q(u) - u| \leq \delta u.$$

Similarly for $u \leq -u_{\min}$, we can also get $|q(u) - u| \leq \delta u$. Thus, Equation (10) is proved. For $u \leq u_{\min}$, $q(u) = 0$ is defined in Equation (9), which implies the results in Equation (11). This completes the proof. □

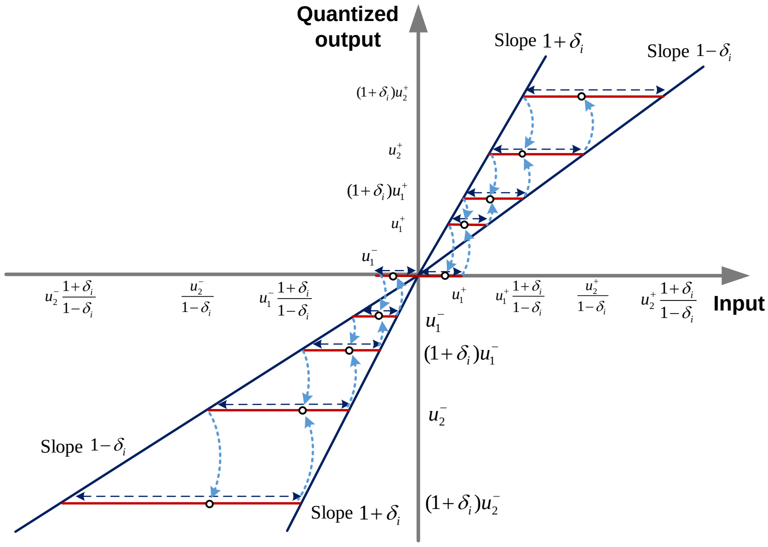

Figure 2. Schematic diagram of hysteresis quantization signal.

3. Coordination Control Design

In this section, the coordination control design is presented. Utilizing the typical cascaded structure of AUV, we use a back-stepping method to design the controller, which allows us to achieve control design for kinematics and dynamics separately.

3.1. Kinematic Control Design

Firstly, we consider the kinematic equation of the ith AUV, $\boldsymbol{\nu}_{1i}$ and $\boldsymbol{\nu}_{2i}$ are used as direct controls to achieve the desired position and attitude of AUV i. We define the position and attitude errors, respectively, as

$$\boldsymbol{e}_{1i} = \boldsymbol{\eta}_{1i} - \boldsymbol{\eta}_{1d} - \boldsymbol{d}_i, \tag{12}$$

$$\boldsymbol{e}_{2i} = \boldsymbol{\eta}_{2i} - \boldsymbol{\eta}_{2id}, \tag{13}$$

where d_i is a constant that is defined based on the desired formation pattern. Then, we define

$$\boldsymbol{e}_{\nu 1i} = \boldsymbol{\nu}_{1i} - \boldsymbol{\alpha}_{\nu 1i}, \tag{14}$$

$$\boldsymbol{e}_{\nu 2i} = \boldsymbol{\nu}_{2i} - \boldsymbol{\alpha}_{\nu 2i}, \tag{15}$$

where $\boldsymbol{\alpha}_{\nu 1i}$ and $\boldsymbol{\alpha}_{\nu 2i}$ are virtual controls which are designed later. According to Equation (1), we have

$$\dot{\boldsymbol{\eta}}_{1i} = \boldsymbol{R}_B^I(\boldsymbol{\eta}_{2i})\boldsymbol{\alpha}_{\nu 1i} + \boldsymbol{\Delta}_i, \tag{16}$$

where $\boldsymbol{\Delta}_i = \boldsymbol{R}_B^I(\boldsymbol{\eta}_{2i})\boldsymbol{e}_{\nu 1i}$. It can be seen that the actual position of the AUV i can be controlled by designing an appropriate virtual control input signal $\boldsymbol{\alpha}_{\nu 1i}$. To this end, we define $\boldsymbol{\varpi}_i = \boldsymbol{R}_B^I(\boldsymbol{\eta}_{2i})\boldsymbol{\alpha}_{\nu 1i}$ and design it as

$$\boldsymbol{\varpi}_i = -k_{e1}\boldsymbol{e}_{1i} - \sum_{j\in\mathcal{N}_i}(\boldsymbol{e}_{1i} - \boldsymbol{e}_{1j}) + \dot{\boldsymbol{\eta}}_{1d}, \tag{17}$$

where k_{e1} is a positive constant, $\dot{\boldsymbol{\eta}}_{1d}$ is the derivative of the desired trajectory $\boldsymbol{\eta}_{1d}$. So virtual control $\boldsymbol{\alpha}_{\nu 1i}$ can be obtained

$$\boldsymbol{\alpha}_{\nu 1i} = \boldsymbol{R}_I^B(-k_{e1}\boldsymbol{e}_{1i} - \sum_{j\in\mathcal{N}_i}(\boldsymbol{e}_{1i} - \boldsymbol{e}_{1j}) + \dot{\boldsymbol{\eta}}_{1d}), \tag{18}$$

Note that the desired reference trajectory information $\boldsymbol{\eta}_{1d}$ and $\dot{\boldsymbol{\eta}}_{1d}$ is used in the virtual control design (18), which is contrary to distributed control design. Thus, the following distributed observer is proposed to estimate the reference position $\boldsymbol{\eta}_{1d}$,

$$\begin{aligned}\dot{\hat{\boldsymbol{\eta}}}_{1di} =& -\sum_{j\in\mathcal{N}_i} k_{ij}(t)a_{ij}(t)sign(\hat{\boldsymbol{\eta}}_{1di}-\hat{\boldsymbol{\eta}}_{1dj}) \\ &- k_i(t)b_i(t)sign(\hat{\boldsymbol{\eta}}_{1di}-\boldsymbol{\eta}_{1d}), \qquad (19)\\ \dot{k}_{ij} =& \nu\left\|\hat{\boldsymbol{\eta}}_{1di}-\hat{\boldsymbol{\eta}}_{1dj}\right\|_1, \dot{k}_i = \nu\|\hat{\boldsymbol{\eta}}_{1di}-\boldsymbol{\eta}_{1d}\|_1, \qquad (20)\end{aligned}$$

where $\mathcal{N}_i := \{j \in \mathcal{V} : (i,j) \in \mathcal{E}\}$, $\hat{\boldsymbol{\eta}}_{1di}$ is the estimate of $\boldsymbol{\eta}_{1d}$ by agent i, $b_i(t)$ is the pinning gain for $i = 1,\ldots,N$ that can access to the reference state. $\|z\|_1$ is the 1-norm of vector $z \in \mathbb{R}^n$, $k_{ij}(t)$ and $k_i(t)$ are adaptive weights, and $\nu \in \mathbb{R}_+$ is a positive control gain. Similarly, the reference velocity $\dot{\boldsymbol{\eta}}_{1d}$ can be estimated by

$$\begin{aligned}\ddot{\hat{\boldsymbol{\eta}}}_{1di} =& -\sum_{j\in\mathcal{N}_i} k_{ij}(t)a_{ij}(t)sign(\dot{\hat{\boldsymbol{\eta}}}_{1di}-\dot{\hat{\boldsymbol{\eta}}}_{1dj}) \\ &- k_i(t)b_i(t)sign(\dot{\hat{\boldsymbol{\eta}}}_{1di}-\dot{\boldsymbol{\eta}}_{1d}), \qquad (21)\\ \dot{k}_{ij} =& \nu\left\|\dot{\hat{\boldsymbol{\eta}}}_{1di}-\dot{\hat{\boldsymbol{\eta}}}_{1dj}\right\|_1, \dot{k}_i = \nu\|\dot{\hat{\boldsymbol{\eta}}}_{1di}-\dot{\boldsymbol{\eta}}_{1d}\|_1, \qquad (22)\end{aligned}$$

where the parameters are defined as same to the above. Then, the following lemma is presented:

Lemma 2. *Under the proposed fully distributed observers (19) and (21) with the adaptive laws (20) and (20) for AUV i, the reference position $\boldsymbol{\eta}_{1d}$ and velocity $\dot{\boldsymbol{\eta}}_{1d}$ can be estimated asymptotically.*

Proof. We define the estimation errors $\tilde{\boldsymbol{\eta}}_{1di} = \hat{\boldsymbol{\eta}}_{1di} - \boldsymbol{\eta}_{1d}$ and $\tilde{\boldsymbol{\eta}}_{1d} = [\tilde{\boldsymbol{\eta}}_{1d1}^\top, \ldots, \tilde{\boldsymbol{\eta}}_{1dn}^\top]^\top$. The error dynamics can be written as … . We choose the Lyapunov function candidate

$$V_o = \frac{1}{2}\tilde{\boldsymbol{\eta}}_{1d}^\top(\mathcal{L}+\mathcal{B})\tilde{\boldsymbol{\eta}}_{1d} + \frac{1}{2\nu}\sum_{i=1}^{n}\sum_{j\in\mathcal{N}_i}(k_{ij}-k_e^*)^2 + \frac{1}{2\nu}\sum_{i=1}^{l}(k_i-k_p^*)^2,$$

where k_e^* and k_p^* are an upper bound on the ideal gains. Taking the time derivative and using the property of the sign function as well as the adaptive laws, we obtain $\dot{V}_o \le -\lambda_{\min}(\mathcal{L}+\mathcal{B})\|\tilde{\boldsymbol{\eta}}_{1d}\|_1 \le 0$. By Barbalat's Lemma, $\tilde{\boldsymbol{\eta}}_{1d} \to 0$, which completes the proof. The velocity observer follows analogously. More detailed proof can also be seen in [20] and is omitted here. □

According to the separation principle, subsequent analysis uses $\boldsymbol{\eta}_{1d}$ and $\dot{\boldsymbol{\eta}}_{1d}$ instead of $\hat{\boldsymbol{\eta}}_{1di}$ and $\dot{\hat{\boldsymbol{\eta}}}_{1di}$ directly.

Then, with the quantified relative information exchange model, the logarithmic quantizer introduced in Equation (7) is considered. Thus, Equation (17) can be rewritten as

$$\boldsymbol{\varpi}_i = -k_{e1}\boldsymbol{e}_{1i} - \sum_{j\in\mathcal{N}_i} Q\left(\boldsymbol{e}_{1i}-\boldsymbol{e}_{1j}\right) + \dot{\boldsymbol{\eta}}_{1d}. \qquad (23)$$

Due to the underlying communication topology among the AUVs, Equation (23) can be written as

$$\boldsymbol{\varpi} = -\boldsymbol{K}_{e1}\boldsymbol{e}_1 - \left(D \otimes I_p\right)\boldsymbol{Q}(\boldsymbol{e}_{cc}) + \dot{\boldsymbol{\eta}}_{1d}, \qquad (24)$$

where $\boldsymbol{L} = D^{\top} D$, $\boldsymbol{e}_{cc} = \left(D^{\top} \otimes I_p\right)\boldsymbol{e}_1$. $\boldsymbol{e}_1$ is concatenation of vectors $\left[\boldsymbol{e}_{11}^{\top}, \ldots, \boldsymbol{e}_{1n}^{\top}\right]^{\top}$. $\boldsymbol{K}_{e1}$ is a diagonal matrix with the values of the elements being k_{e1}. I_p is a suitable identity matrix. Then, we have

$$\dot{\boldsymbol{e}}_1 = -\boldsymbol{K}_{e1}\boldsymbol{e}_1 - (D \otimes I_p)Q(\boldsymbol{e}_{cc}) + \left(\boldsymbol{\Delta}_i \otimes I_p\right). \tag{25}$$

For the error dynamics (25), we consider the following Lyapunov function candidate:

$$V_1 = \frac{1}{2}\boldsymbol{e}_{cc}^T \boldsymbol{e}_{cc}. \tag{26}$$

Taking the derivative of Equation (26) along Equation (25) and multiplying $(D^{\top} \otimes I_p)$ on both sides of it, we can get

$$\begin{aligned}
\dot{V}_1 =& \boldsymbol{e}_{cc}^T\left[-\left(D^T D \otimes Ip\right)\boldsymbol{e}_{cc} - \left(D^T D \otimes Ip\right)\varrho(\boldsymbol{e}_{cc})\right] \\
& - \boldsymbol{e}_{cc}^T \boldsymbol{K}_{e1}\boldsymbol{e}_{cc} + \sum_{i=1}^{n} \sum_{i \neq j, j \in \mathcal{N}_i} Q\left(\boldsymbol{e}_{1i} - \boldsymbol{e}_{1j}\right)^T \boldsymbol{\Delta}_i \\
\leq& -(k_{e1} + \lambda_{\min}(\boldsymbol{L}))\|\boldsymbol{e}_{cc}\|^2 + \sigma\lambda_{\max}(\boldsymbol{L})\|\boldsymbol{e}_{cc}\|^2 \\
& + \sum_{i=1}^{n} \sum_{i \neq j, j \in \mathcal{N}_i} Q\left(\boldsymbol{e}_{1i} - \boldsymbol{e}_{1j}\right)^T \boldsymbol{\Delta}_i,
\end{aligned} \tag{27}$$

where $\varrho(\boldsymbol{e}_{cc}) = Q(\boldsymbol{e}_{cc}) - \boldsymbol{e}_{cc}$. Choosing the appropriate logarithmic quantizer parameters in Equation (7) as follows

$$\sigma < \frac{k_{e1} + \lambda_{\min}(\boldsymbol{L})}{\lambda_{\max}(\boldsymbol{L})}, \tag{28}$$

and defining

$$l = -(k_{e1} + \lambda_{\min}(\boldsymbol{L})) + \sigma\lambda_{\max}(\boldsymbol{L}) < 0, \tag{29}$$

Equation (27) can be rewritten as

$$\dot{V}_1 \leq 2lV_1 + \sum_{i=1}^{n} \sum_{i \neq j, j \in \mathcal{N}_i} Q\left(\boldsymbol{e}_{1i} - \boldsymbol{e}_{1j}\right)^T \boldsymbol{\Delta}_i. \tag{30}$$

In addition, the virtual control $\boldsymbol{\alpha}_{v2i}$ is designed as

$$\boldsymbol{\alpha}_{v2i} = -k_{e2i}\boldsymbol{T}(\boldsymbol{\eta}_{2i})\boldsymbol{e}_{2i} + \boldsymbol{T}(\boldsymbol{\eta}_{2i})\dot{\boldsymbol{\eta}}_{2id}, \tag{31}$$

where k_{e2i} is positive control gain and $\dot{\boldsymbol{\eta}}_{2id}$ is the derivative of desired attitude of AUV i. Note that the desired attitude $\boldsymbol{\eta}_{2id}$ and its derivative $\dot{\boldsymbol{\eta}}_{2id}$ is specified for each AUV. If not, they can also be obtained by using the similar distributed adaptive observer as shown in (19) and (20).

Then, the following Lyapunov function is chosen for the error dynamics of $\boldsymbol{e}_{2i}$,

$$V_2 = \frac{1}{2}\sum_{i=1}^{n} \boldsymbol{e}_{2i}^T \boldsymbol{e}_{2i}, \tag{32}$$

and its derivative is given as

$$\dot{V}_2 \leq \sum_{i=1}^{n} \boldsymbol{e}_{2i}^{\mathrm{T}}\left(\boldsymbol{T}^{-1}(\boldsymbol{\eta}_{2i})\boldsymbol{\alpha}_{v2i} + \boldsymbol{T}^{-1}(\boldsymbol{\eta}_{2i})\boldsymbol{e}_{v2i} - \dot{\boldsymbol{\eta}}_{2id}\right). \tag{33}$$

Then, combining (31) into (33) yields

$$\begin{aligned}\dot{V}_2 &\leq \sum_{i=1}^{n} \boldsymbol{e}_{2i}^{\mathrm{T}} \Big(\boldsymbol{T}^{-1}(\boldsymbol{\eta}_{2i})\boldsymbol{\alpha}_{v2i} + \boldsymbol{T}^{-1}(\boldsymbol{\eta}_{2i})\boldsymbol{e}_{v2i} - \dot{\boldsymbol{\eta}}_{2id} \Big) \\ &\leq -k_{e2i} \sum_{i=1}^{n} \boldsymbol{e}_{2i}^{T}\boldsymbol{e}_{2i} + \sum_{i=1}^{n} \boldsymbol{e}_{2i}^{\mathrm{T}} \boldsymbol{T}^{-1}(\boldsymbol{\eta}_{2i})\boldsymbol{e}_{v2i} \\ &= -2k_{e2i}V_2 + \sum_{i=1}^{n} \boldsymbol{e}_{2i}^{\mathrm{T}} \boldsymbol{T}^{-1}(\boldsymbol{\eta}_{2i})\boldsymbol{e}_{v2i}. \end{aligned} \tag{34}$$

In this stage, the kinematic design of the AUV is completed, and we obtain suitable virtual controls $\boldsymbol{e}_{v1i}$ and $\boldsymbol{e}_{v2i}$. In the following control design, a suitable controller is designed for the dynamics model of AUVs to compensate the second terms in (30) and (34).

3.2. Dynamics Control Design

According to the property of the quantizer as shown in Lemma 1, Equation (3) can be rewritten as

$$\boldsymbol{M}_i\dot{\boldsymbol{\nu}}_i + \boldsymbol{C}_i(\boldsymbol{\nu}_i)\boldsymbol{\nu}_i + \boldsymbol{D}_i(\boldsymbol{\nu}_i)\boldsymbol{\nu}_i + \boldsymbol{g}_i = \boldsymbol{\tau}_i + \boldsymbol{\mu}_i. \tag{35}$$

We define $\boldsymbol{e}_{vi} = [\boldsymbol{e}_{v1i}^{\top}, \boldsymbol{e}_{v2i}^{\top}]^{\top}$ and $\boldsymbol{\alpha}_{vi} = [\boldsymbol{\alpha}_{vi}^{\top}, \boldsymbol{\alpha}_{vi}^{\top}]^{\top}$. The errors in Equations (14) and (15) can be rewritten as $\boldsymbol{e}_{vi} = \boldsymbol{\nu}_i - \boldsymbol{\alpha}_{vi}$. Then, the control law is designed as

$$\begin{aligned}\boldsymbol{\tau}_i = {}& (\boldsymbol{M}_i\dot{\boldsymbol{\alpha}}_{vi} + \boldsymbol{C}_i(\boldsymbol{\nu}_i)\boldsymbol{\nu}_i + \boldsymbol{D}_i(\boldsymbol{\nu}_i)\boldsymbol{\nu}_i + \boldsymbol{g}_i - k_{evi}\boldsymbol{e}_{vi} \\ & - \left[\sum_{i\neq j, j\in\mathcal{N}_i} Q\big(\boldsymbol{e}_{1i} - \boldsymbol{e}_{1j}\big)^{T} \boldsymbol{R}_B^I \quad \boldsymbol{e}_{2i}^{\mathrm{T}}\boldsymbol{T}^{-1}(\boldsymbol{\eta}_{2i}) \right]^{\top} \\ & + \tanh\Big(\frac{\boldsymbol{e}_{vi}}{\varepsilon}\Big) \odot \boldsymbol{\tau}_{i\,\min}\,) \oslash \Big(\delta \tanh\Big(\frac{\boldsymbol{e}_{vi}\odot\boldsymbol{\tau}_i}{\varepsilon}\Big) + \mathbf{1}\Big)\end{aligned} \tag{36}$$

where k_{evi} is a positive control gain, $\tanh(\cdot)$ is hyperbolic tangent function, $\boldsymbol{A}\odot\boldsymbol{B} = [a_{ij}b_{ij}]$ and $\boldsymbol{A}\oslash\boldsymbol{B} = [\frac{a_{ij}}{b_{ij}}]$ with $\boldsymbol{A} = [a_{ij}]$ and $\boldsymbol{B} = [b_{ij}]$ being matrices with the same dimension, $\mathbf{1} = [1,1,1,1,1,1]^{\mathrm{T}}$.

Remark 3. *The proposed control strategy is fully distributed, and each AUV computes its control input using only local state information and quantized relative measurements received from neighboring agents. Therefore, the computational complexity of each AUV mainly depends on its local degree rather than the total number of vehicles in the network. Specifically, the controller consists of algebraic feedback terms, adaptive parameter updates, and element-wise quantization compensation, all of which are lightweight and suitable for real-time embedded implementation. When the total number of AUVs increases while the communication graph remains sparse, the per-agent computational burden remains nearly unchanged. From the communication perspective, only neighbor-to-neighbor information exchange is required, and the use of quantized signals further reduces the communication payload. This property is particularly beneficial for bandwidth-limited underwater acoustic channels. Nevertheless, in dense communication networks where each AUV interacts with many neighbors, the communication overhead, synchronization burden, and packet collision probability may increase. In such cases, the practical bottleneck is mainly communication rather than controller computation. Therefore, for large-scale formations, sparse but connected topologies, such as nearest-neighbor graphs, leader–follower structures, ring networks, or spanning-tree-based architectures, are generally more suitable. These topologies preserve cooperative performance while significantly reducing network load.*

Theorem 1. *Given a connected AUV networks modeled by Equations (1)–(3), under the proposed control law (36) with the quantizer parameter σ satisfying (28), the control objectives in (4)–(6) can be achieved with* $\delta = \sqrt{\frac{\kappa}{\beta_i}}$, $\beta_i = \min\{l, 2k_{e2i}, 2\epsilon_i\}$, $\kappa = 0.2785\varepsilon \sum_{i=1}^{n}(\boldsymbol{\tau}_{i\,\min}) + 1.671\delta\varepsilon n$.

Proof. We consider the following Lyapunov function:

$$V_3 = V_1 + V_2 + \frac{1}{2}\sum_{i=1}^{n} \boldsymbol{e}_{vi}^T M_i \boldsymbol{e}_{vi} \tag{37}$$

Taking the time derivative of V_3 along the closed-loop error dynamics gives

$$\begin{aligned}\dot{V}_3 =& \dot{V}_1 + \dot{V}_2 + \sum_{i=1}^{n} \boldsymbol{e}_{vi}^\top M_i \dot{\boldsymbol{e}}_{vi} + \frac{1}{2}\sum_{i=1}^{n} \boldsymbol{e}_{vi}^\top \dot{M}_i \boldsymbol{e}_{vi}\\ \leq& 2lV_1 - k_{e2i}\sum_{i=1}^{n} \boldsymbol{e}_{2i}^\top \boldsymbol{e}_{2i} + \sum_{i=1}^{n} \boldsymbol{e}_{2i}^\top T^{-1}(\boldsymbol{\eta}_{2i})\boldsymbol{e}_{v2i}\\ &+ \sum_{i=1}^{n}\sum_{\substack{j\in\mathcal{N}_i\\ j\neq i}} Q(\boldsymbol{e}_{1i} - \boldsymbol{e}_{1j})^\top R_B^I(\boldsymbol{\eta}_{2i})\boldsymbol{e}_{v1i}\\ &+ \sum_{i=1}^{n} \boldsymbol{e}_{vi}^\top M_i(\dot{\boldsymbol{v}}_i - \dot{\alpha}_{vi}) + \frac{1}{2}\sum_{i=1}^{n} \boldsymbol{e}_{vi}^\top \dot{M}_i \boldsymbol{e}_{vi}.\end{aligned} \tag{38}$$

By using the AUV dynamics

$$M_i\dot{\boldsymbol{v}}_i = q(\tau_i) - C_i(\boldsymbol{v}_i)\boldsymbol{v}_i - D_i(\boldsymbol{v}_i)\boldsymbol{v}_i - g_i,$$

and the skew-symmetric property $\dot{M}_i - 2C_i(\boldsymbol{v}_i)$, one has

$$\begin{aligned}\dot{V}_3 \leq& 2lV_1 - k_{e2i}\sum_{i=1}^{n} \boldsymbol{e}_{2i}^\top \boldsymbol{e}_{2i}\\ &+ \sum_{i=1}^{n} \boldsymbol{e}_{vi}^\top [q(\tau_i) - C_i(\boldsymbol{v}_i)\boldsymbol{v}_i - D_i(\boldsymbol{v}_i)\boldsymbol{v}_i - g_i - M_i\dot{\alpha}_{vi}]\\ &+ \sum_{i=1}^{n} \boldsymbol{e}_{vi}^\top \Xi_i,\end{aligned} \tag{39}$$

where

$$\Xi_i = \begin{bmatrix} \sum\limits_{\substack{j\in\mathcal{N}_i\\ j\neq i}} R_I^B(\boldsymbol{\eta}_{2i})Q(\boldsymbol{e}_{1i} - \boldsymbol{e}_{1j}) \\ T^{-\top}(\boldsymbol{\eta}_{2i})\boldsymbol{e}_{2i} \end{bmatrix}. \tag{40}$$

Since the hysteresis quantizer satisfies

$$q(\tau_i) = \tau_i + \mu_i, \tag{41}$$

it follows that

$$\boldsymbol{e}_{vi}^\top q(\tau_i) = \boldsymbol{e}_{vi}^\top \tau_i + \boldsymbol{e}_{vi}^\top \mu_i. \tag{42}$$

For the kth component, Lemma 1 gives

$$|\mu_{i,k}| \leq \delta|\tau_{i,k}|, \quad |\tau_{i,k}| \geq \tau_{i\,\min},$$

and

$$|\mu_{i,k}| \leq \tau_{i\,\min}, \quad |\tau_{i,k}| \leq \tau_{i\,\min}.$$

Therefore, the quantization error term can be upper bounded as

$$\begin{aligned} \boldsymbol{e}_{vi}^{\top}\mu_i &= \sum_{k=1}^{6} \boldsymbol{e}_{vi,k}\mu_{i,k} \\ &\leq \sum_{k=1}^{6} |\boldsymbol{e}_{vi,k}|\,|\mu_{i,k}| \\ &\leq \sum_{k=1}^{6} |\boldsymbol{e}_{vi,k}|\tau_{i\,\min} + \delta \sum_{k=1}^{6} |\boldsymbol{e}_{vi,k}|\,|\tau_{i,k}|. \end{aligned} \tag{43}$$

Thus,

$$\boldsymbol{e}_{vi}^{\top} q(\tau_i) \leq \boldsymbol{e}_{vi}^{\top}\tau_i + \sum_{k=1}^{6} |\boldsymbol{e}_{vi,k}|\tau_{i\,\min} + \delta \sum_{k=1}^{6} |\boldsymbol{e}_{vi,k}|\,|\tau_{i,k}|. \tag{44}$$

To handle the nonsmooth absolute-value terms, the following smooth approximation inequality is used:

$$0 \leq |\rho| - \rho \tanh\left(\frac{\rho}{\varepsilon}\right) \leq 0.2785\varepsilon, \quad \varepsilon > 0. \tag{45}$$

By applying (45) to $\rho = \boldsymbol{e}_{vi,k}$ and $\rho = \boldsymbol{e}_{vi,k}\tau_{i,k}$, one obtains

$$|\boldsymbol{e}_{vi,k}|\tau_{i\,\min} \leq \boldsymbol{e}_{vi,k} \tanh\left(\frac{\boldsymbol{e}_{vi,k}}{\varepsilon}\right)\tau_{i\,\min} + 0.2785\varepsilon\tau_{i\,\min}, \tag{46}$$

$$|\boldsymbol{e}_{vi,k}|\,|\tau_{i,k}| = |\boldsymbol{e}_{vi,k}\tau_{i,k}| \leq \boldsymbol{e}_{vi,k}\tau_{i,k} \tanh\left(\frac{\boldsymbol{e}_{vi,k}\tau_{i,k}}{\varepsilon}\right) + 0.2785\varepsilon. \tag{47}$$

Substituting (46) and (47) into (44) yields

$$\begin{aligned} \boldsymbol{e}_{vi}^{\top} q(\tau_i) \leq \boldsymbol{e}_{vi}^{\top}\tau_i &+ \boldsymbol{e}_{vi}^{\top}\left[\tanh\left(\frac{\boldsymbol{e}_{vi}}{\varepsilon}\right) \odot \tau_{i\,\min}\mathbf{1}\right] \\ &+ \delta \boldsymbol{e}_{vi}^{\top}\left[\tanh\left(\frac{\boldsymbol{e}_{vi} \odot \tau_i}{\varepsilon}\right) \odot \tau_i\right] \\ &+ 0.2785\varepsilon \sum_{k=1}^{6} \tau_{i\,\min} + 6 \times 0.2785\delta\varepsilon. \end{aligned} \tag{48}$$

The above inequality shows that the quantization-induced terms can be compensated by introducing the corresponding hyperbolic-tangent terms. Therefore, the actual control input is designed as

$$\begin{aligned} \tau_i = M_i\dot{\alpha}_{v_i} + C_i(\boldsymbol{\nu}_i)\nu_i + D_i(\boldsymbol{\nu}_i)\boldsymbol{\nu}_i + g_i - \Xi_i - k_{evi}\boldsymbol{e}_{vi} \\ - \tanh\left(\frac{\boldsymbol{e}_{vi}}{\varepsilon}\right) \odot \tau_{i\,\min}\mathbf{1} - \delta \tanh\left(\frac{\boldsymbol{e}_{vi} \odot \tau_i}{\varepsilon}\right) \odot \tau_i, \end{aligned} \tag{49}$$

where $k_{evi} > 0$ and $\mathbf{1} = [1,1,1,1,1,1]^{\top}$. Substituting (49) into (39) and using (48), one obtains

$$\dot{V}_3 \leq 2lV_1 - k_{e2i}\sum_{i=1}^{n} \boldsymbol{e}_{2i}^{\top}\boldsymbol{e}_{2i} - k_{evi}\sum_{i=1}^{n} \boldsymbol{e}_{vi}^{\top}\boldsymbol{e}_{vi} + \kappa, \tag{50}$$

where

$$\kappa = 0.2785\varepsilon \sum_{i=1}^{n}\sum_{k=1}^{6} \tau_{i\,\min} + 1.671\delta\varepsilon n. \tag{51}$$

Since $l < 0$, it follows that

$$2lV_1 = -2|l|V_1. \tag{52}$$

Hence, (50) can be rewritten as

$$\dot{V}_3 \leq -2|l|V_1 - k_{e2i}\sum_{i=1}^{n} \boldsymbol{e}_{2i}^{\top}\boldsymbol{e}_{2i} - k_{evi}\sum_{i=1}^{n} \boldsymbol{e}_{vi}^{\top}\boldsymbol{e}_{vi} + \kappa. \tag{53}$$

Furthermore, since M_i is positive definite, there exist positive constants $\underline{m}_i$ and $\overline{m}_i$ such that

$$\underline{m}_i\|\boldsymbol{e}_{vi}\|^2 \leq \boldsymbol{e}_{vi}^{\top}M_i\boldsymbol{e}_{vi} \leq \overline{m}_i\|\boldsymbol{e}_{vi}\|^2.$$

Therefore, there exists a positive constant β such that

$$\dot{V}_3 \leq -\beta V_3 + \kappa, \tag{54}$$

where

$$\beta = \min\left\{2|l|, 2k_{e2i}, \frac{2k_{evi}}{\overline{m}_i}\right\}, \tag{55}$$

where $\bar{m} = \max_i \lambda_{\max}(M_i)$ and

$$l = -(k_{e1} + \lambda_{\min}(L)) + \sigma\lambda_{\max}(L) < 0. \tag{56}$$

Solving (54) gives

$$V_3(t) \leq \boldsymbol{e}^{-\beta t}V_3(0) + \frac{\kappa}{\beta}\left(1 - e^{-\beta t}\right). \tag{57}$$

Thus, all closed-loop signals are uniformly ultimately bounded, and

$$\limsup_{t\to\infty} V_3(t) \leq \frac{\kappa}{\beta}. \tag{58}$$

Consequently, the formation tracking errors converge to an adjustable neighborhood of zero. Moreover, the ultimate bound can be reduced by appropriately selecting the quantization parameters $\tau_{i\,\min}$, δ, and the smooth approximation parameter ε.

In addition, the measurement quantization parameter σ affects the ultimate bound through the decay-rate-related term $|l|$, while the input quantization parameter δ directly affects the residual term κ. Since

$$V_3 = V_1 + V_2 + \frac{1}{2}\sum_{i=1}^{n} \boldsymbol{e}_{vi}^{\top}M_i\boldsymbol{e}_{vi}, \tag{59}$$

the tracking errors satisfy

$$\limsup_{t\to\infty} \|\boldsymbol{e}_{cc}(t)\| \leq \sqrt{\frac{2\kappa}{\beta}}, \tag{60}$$

$$\limsup_{t\to\infty}\left(\sum_{i=1}^{n}\|\boldsymbol{e}_{2i}(t)\|^2\right)^{1/2} \leq \sqrt{\frac{2\kappa}{\beta}}, \tag{61}$$

$$\limsup_{t\to\infty}\left(\sum_{i=1}^{n}\|\boldsymbol{e}_{vi}(t)\|^2\right)^{1/2} \leq \sqrt{\frac{2\kappa}{\beta\underline{m}}}, \tag{62}$$

where $\underline{m} = \min_i \lambda_{\min}(M_i)$. Equations (60)–(62) explicitly show that the ultimate tracking accuracy can be improved by decreasing the quantization parameters σ and δ, decreasing the smoothing parameter ε, or increasing the control gains k_{e1}, k_{e2}, and k_{ev}, provided that the actuator limits and implementation constraints are respected. This completes the proof. □

Remark 4. *For the selection of quantizer parameters σ and δ, as long as Equation (28) is satisfied, the parameter selection is arbitrary. So Equation (28) can quantify the guidance of the device parameters. Since the input signal τ_i is bounded and δ is also bounded, the required number of quantization levels of the hysteretic quantizer is finite.*

Remark 5. *The above ultimate bounds are theoretical worst-case estimates. They are obtained by using norm inequalities, the sector bounds of the quantizer, and the smooth approximation inequality $0 \le |\rho| - \rho \tanh(\rho/\varepsilon) \le 0.2785\varepsilon$. Therefore, the bounds are generally conservative. In practical simulations, the actual steady-state tracking errors are usually smaller than the analytical upper bounds because the quantization error does not always attain its worst-case value and the signs of different error components may partially cancel each other.*

3.3. The Impact of Observer Convergence Speed

The distributed observers in (19) and (21) are introduced to estimate the desired reference position and velocity using only local communication. We define the estimation errors as

$$\tilde{\boldsymbol{\eta}}_{1di} = \hat{\boldsymbol{\eta}}_{1di} - \boldsymbol{\eta}_{1d}, \qquad \dot{\tilde{\boldsymbol{\eta}}}_{1di} = \dot{\hat{\boldsymbol{\eta}}}_{1di} - \dot{\boldsymbol{\eta}}_{1d}. \tag{63}$$

When the estimated signals are used in the virtual controller, the kinematic control law becomes

$$\varpi_i = -k_{e1}\boldsymbol{e}_{1i} - \sum_{j\in\mathcal{N}_i} Q(\boldsymbol{e}_{1i} - \boldsymbol{e}_{1j}) + \dot{\boldsymbol{\eta}}_{1d} + \Delta_{oi}, \tag{64}$$

where the observer-induced perturbation term is $\Delta_{oi} = \dot{\tilde{\boldsymbol{\eta}}}_{1di} - k_{e1}\tilde{\boldsymbol{\eta}}_{1di}$. Accordingly, the Lyapunov derivative contains an additional term $\boldsymbol{e}_{cc}^{\top}\Delta_o$ with Δ_o being the stacked observer error vector. Using Young's inequality, for any $\mu > 0$,

$$\boldsymbol{e}_{cc}^{\top}\Delta_o \le \frac{\mu}{2}\|\boldsymbol{e}_{cc}\|^2 + \frac{1}{2\mu}\|\Delta_o\|^2. \tag{65}$$

Hence, the closed-loop derivative can be written as

$$\dot{V}_3 \le -\beta_o V_3 + \kappa_o + \frac{1}{2\mu}\|\Delta_o\|^2, \tag{66}$$

where $\beta_o = \beta - \mu$, $0 < \mu < \beta$. Therefore, if the observer errors are bounded, then all closed-loop signals remain bounded. If

$$\lim_{t\to\infty} \Delta_o(t) = 0, \tag{67}$$

then the observer perturbation asymptotically vanishes and the original tracking result of Theorem 1 is recovered. Moreover, if the observer satisfies exponential convergence

$$\|\Delta_o(t)\| \le c_o e^{-\lambda_o t}, \tag{68}$$

where $c_o > 0$ and $\lambda_o > 0$, then larger λ_o implies faster estimation convergence, smaller transient tracking errors, and shorter formation synchronization time.

Remark 6. *Observer errors do not destabilize the closed-loop system provided that the communication graph satisfies the observer connectivity condition and the observer gains are selected such that the estimation dynamics are stable. However, excessively slow observer convergence or prolonged communication loss may enlarge transient tracking errors and degrade convergence speed. Therefore, in practical implementation, the observer bandwidth should be chosen sufficiently larger than the dominant closed-loop tracking bandwidth.*

https://doi.org/10.3390/electronics15102050

3.4. Robustness Against Disturbances and Measurement Noise

In practical AUV systems, unmodeled hydrodynamics, ocean currents, and measurement noise are unavoidable. To discuss the robustness of the proposed controller, the AUV dynamics can be rewritten as

$$M_i\dot{\boldsymbol{v}}_i + C_i(\boldsymbol{v}_i)\boldsymbol{v}_i + D_i(\boldsymbol{v}_i)\boldsymbol{v}_i + g_i = q(\tau_i) + d_i(t), \tag{69}$$

where $d_i(t) \in \mathbb{R}^6$ denotes the lumped disturbance including unmodeled dynamics, ocean-current-induced forces, and bounded measurement noise effects. It is assumed that

$$\|d_i(t)\| \le \bar{d}_i, \tag{70}$$

where $\bar{d}_i > 0$ is an unknown but bounded constant. Following the same Lyapunov analysis as in Theorem 1, the derivative of V_3 contains an additional term

$$\sum_{i=1}^{n} \boldsymbol{e}_{vi}^{\top} d_i(t). \tag{71}$$

By Young's inequality, for any $\chi_i > 0$, one has

$$\boldsymbol{e}_{vi}^{\top} d_i(t) \le \frac{\chi_i}{2}\|\boldsymbol{e}_{vi}\|^2 + \frac{1}{2\chi_i}\bar{d}_i^2. \tag{72}$$

Therefore, the Lyapunov derivative satisfies

$$\dot{V}_3 \le -\beta_d V_3 + \kappa_d, \tag{73}$$

where

$$\beta_d = \min\left\{2|l|, 2k_{e2}, \frac{2(k_{ev} - \chi/2)}{\bar{m}}\right\}, \tag{74}$$

$$\kappa_d = \kappa + \sum_{i=1}^{n} \frac{\bar{d}_i^2}{2\chi_i}, \tag{75}$$

with $\chi = \max_i \chi_i$, $\bar{m} = \max_i \lambda_{\max}(M_i)$, and $k_{ev} > \chi/2$. Hence, all closed-loop signals remain uniformly ultimately bounded and

$$\limsup_{t\to\infty} V_3(t) \le \frac{\kappa_d}{\beta_d}. \tag{76}$$

It can be observed from (76) that bounded disturbances and measurement noise enlarge the ultimate bound but do not destroy closed-loop boundedness. The disturbance attenuation capability can be improved by increasing the velocity feedback gain k_{ev}, provided that actuator constraints are satisfied.

Remark 7. *The above analysis shows that the proposed controller is robust against bounded unmodeled dynamics, ocean-current disturbances, and measurement noise in the sense of uniform ultimate boundedness. The ultimate tracking accuracy depends on both the quantization-induced residual term κ and the disturbance-dependent term $\sum_{i=1}^{n} \bar{d}_i^2/(2\chi_i)$. Therefore, smaller quantization levels, lower measurement noise, and larger stabilizing gains lead to improved steady-state tracking performance.*

4. Simulations

In this section, simulation results are presented to verify the effectiveness of the adaptive controller proposed in this paper. Three AUVs are considered in the network, which is given in Figure 3. The Laplacian matrix $\boldsymbol{L}$ and incidence matrix D of the underlying communication topology of this group of AUVs are given as follows:

$$\boldsymbol{L} = D^T D = \begin{pmatrix} 2 & -1 & -1 \\ -1 & 1 & 0 \\ -1 & 0 & 1 \end{pmatrix}, D^T = \begin{pmatrix} 1 & 1 \\ -1 & 0 \\ 0 & -1 \end{pmatrix}$$

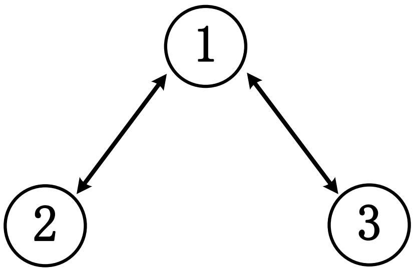

Figure 3. Interaction topology between the AUVs.

Then, the initial positions of the three AUVs are randomly chosen as $\boldsymbol{\eta}_1 = [10, -12, 10, 0, 0, 0]^T$, $\boldsymbol{\eta}_2 = [26, -13, -20, 0, 0, 0]^T$, $\boldsymbol{\eta}_3 = [-11, -5, -10, 0, 0, 0]^T$. We define the desired offsets d relative to the desired track trajectory for the formation pattern of AUVs as $\boldsymbol{R} = [\boldsymbol{d}_1, \boldsymbol{d}_2, \boldsymbol{d}_3]$ with $\boldsymbol{d}_1 = [10, 10, 0]^T$, $\boldsymbol{d}_2 = [10, -10, 0]^T$, $\boldsymbol{d}_3 = [-10, 10, -10]^T$. According to Theorem 1, the suitable control parameters and quantizer parameters are chosen as $k_{e1i} = 0.5$, $k_{e2i} = 1$, $k_{evi} = 1000$, $k_{evi} = 1000$, $\tau_{\min i} = 0.02$, $\sigma = 0.8$, $\delta = 0.2$ for $i = 1, \ldots, 3$.

Then, the simulation results are given in Figures 4–7. Figure 4 plots the spatial paths of AUV1, AUV2, and AUV3 from their random initial positions to the final formation. The desired geometric pattern, which is a triangle defined by the offsets $d_1 = [10, 10, 0]^T$, $d_2 = [10, 110, 0]^T$, $d_3 = [-10, 10, -10]^T$, is superimposed on the trajectories. One can clearly observe that after a short transient, the three AUVs converge to the vertices of the prescribed triangle and maintain this shape while moving and the circumcenter of the triangle follows the desired trajectory $\boldsymbol{\eta}_{1d}$. The three components of the position error $\boldsymbol{e}_{1i} = \boldsymbol{\eta}_{1i} - \boldsymbol{\eta}_{1d} - d_i$ for $i = 1, 2, 3$ are shown in Figure 6. All error signals converge rapidly from initial values on the order of tens of meters to a small neighborhood around zero. The steady-state errors remain within a band of less than 0.05 m, which is well within the adjustable neighborhood δ promised by Theorem 1. Additionally, the inter-vehicle relative position errors $\boldsymbol{\eta}_{1i} - \boldsymbol{\eta}_{1j} - (d_i - d_j)$ are directly linked to $\boldsymbol{e}_{1i} - \boldsymbol{e}_{1j}$, as shown in Figure 5. Figure 6 therefore demonstrates that the condition in Equation (4) is met. In Figure 7, the evolution of the attitude error vector $\boldsymbol{e}_{2i} = \boldsymbol{\eta}_{2i} - \boldsymbol{\eta}_{2id}$ for each AUV are displayed. The roll, pitch, and yaw error components all converge to a region near zero within a few seconds. The final attitude tracking errors are bounded by 0.02rad, which satisfies the requirement $\|\boldsymbol{\eta}_{2i} - \boldsymbol{\eta}_{2id}\| < \delta$ of Equation (6). Thus, each AUV individually attains its prescribed orientation while participating in the cooperative formation.

It is worth noting that many conventional backstepping-based AUV controllers and cooperative tracking methods are developed under continuous-state measurement and continuous-input assumptions. When directly implemented in the presence of coarse quantization, their theoretical guarantees may no longer hold, since quantization errors enter both the sensing and actuation channels. Compared with such non-quantization-aware designs, the proposed method explicitly incorporates quantized relative measurements into the cooperative control term and introduces a hysteresis-quantizer compensation mechanism for the actuator input. As a result, the closed-loop system admits an analytically characterized ultimate tracking bound whose size can be adjusted through the quantization parameters and controller gains.

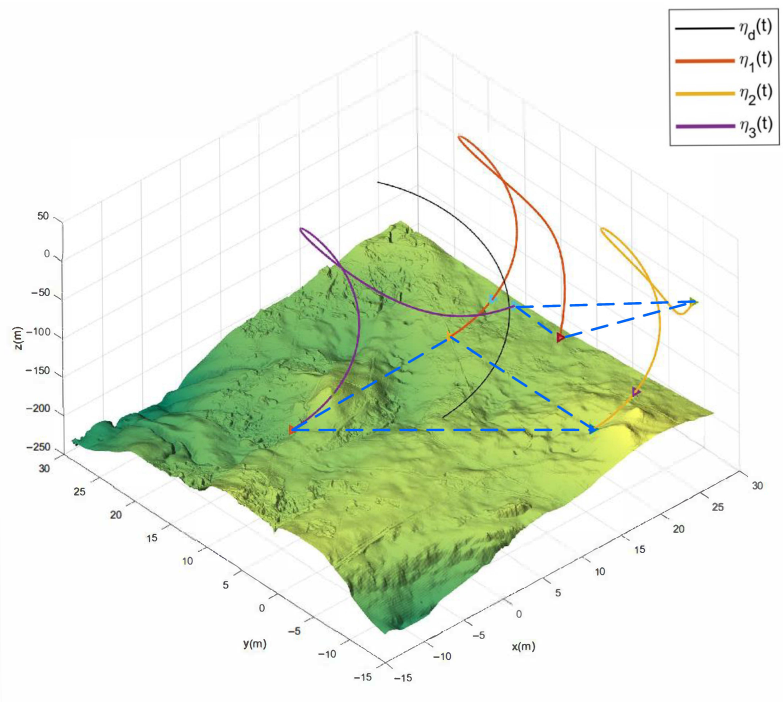

Figure 4. The position of AUVs in the three-dimensional frame.

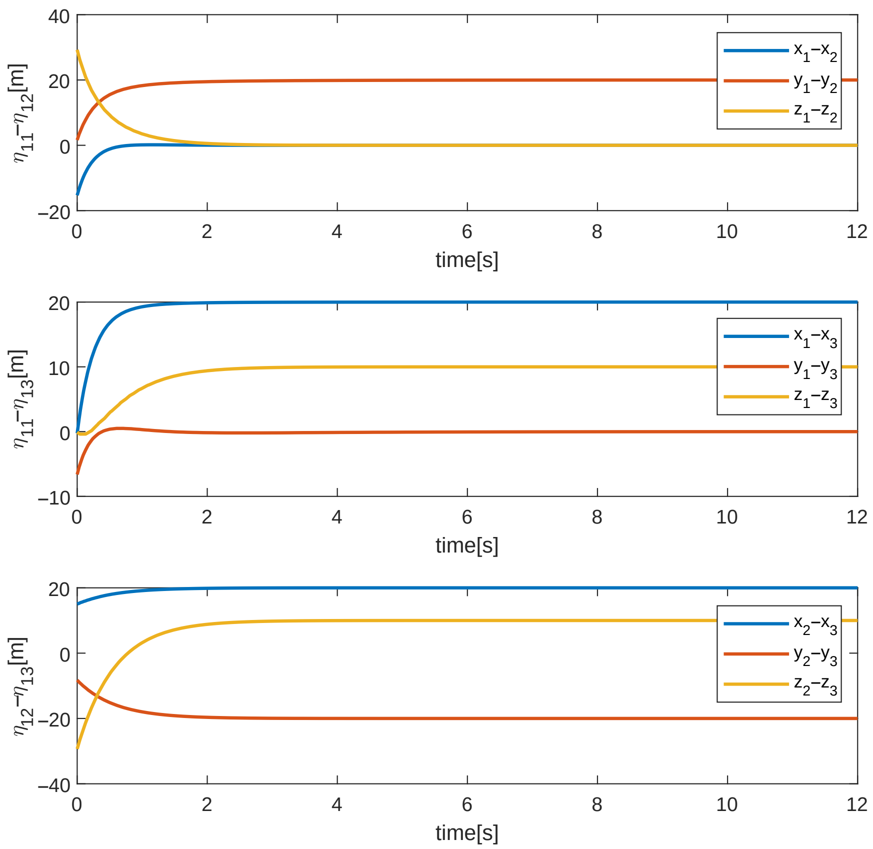

Figure 5. Coordination error $\boldsymbol{\eta}_{1i} - \boldsymbol{\eta}_{1j}$.

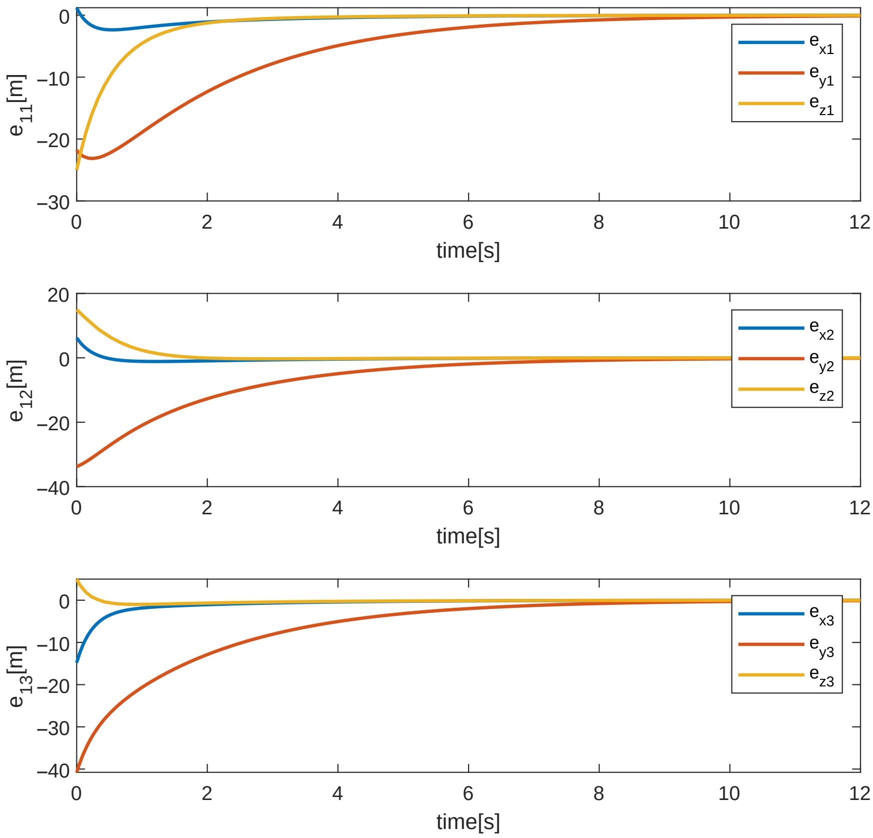

Figure 6. Position error e_{1i} of AUV i.

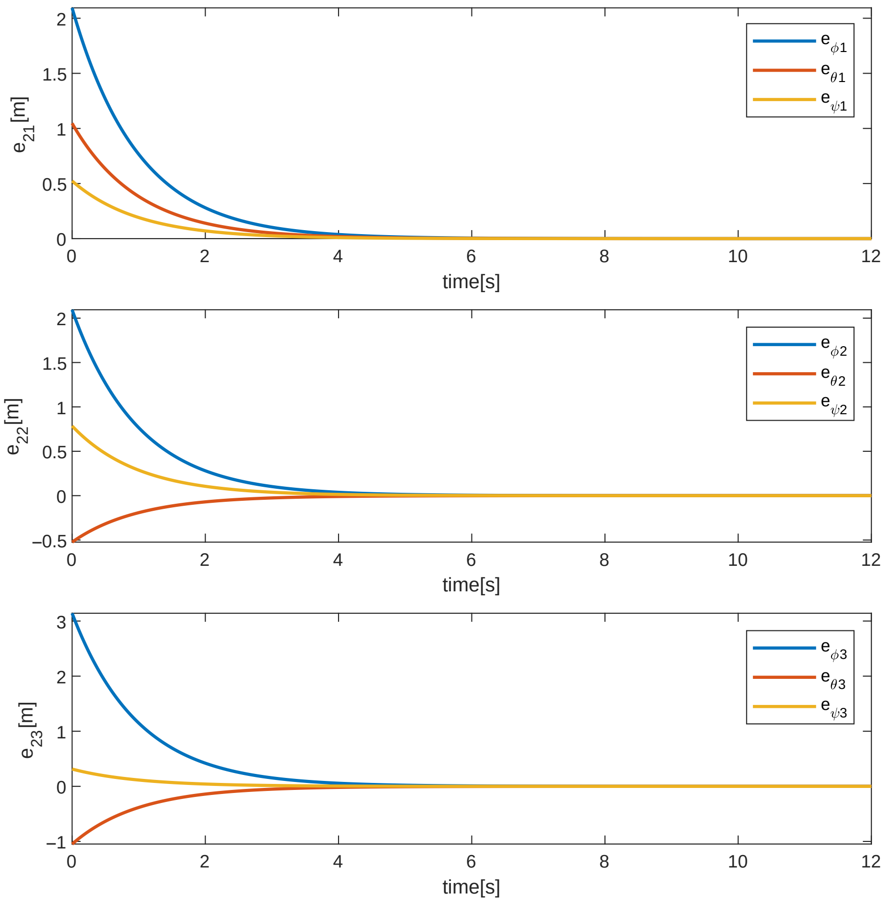

Figure 7. Attitude error e_{2i} of AUV i.

5. Conclusions

This paper studies the cooperative control tracking problem of a group of AUVs based on quantified relative measurements and quantified inputs. A group of AUVs needs to converge, stay within the preset graphics, and complete the tracking task. In order to achieve the control objectives, the backstepping method is used to design the adaptive controller. Quantized relative measurement signals are used to design a quantified consensus algorithm. Based on the nonlinearity of the quantized input signal, the quantization parameters and system gain are selected according to the proposed inequality, which ensures the stability and stable error of the system within the adjustable range. The simulation results prove the effectiveness of the controller designed in this article. The underwater environment is complex and changeable. In order to meet actual control requirements, we can consider actual environmental conditions such as ocean current changes, time delays, and temperature changes in future research [21–24]. In subsequent research, the real ocean environment can be gradually simulated [25]. In addition, future work will consider scalable extensions including event-triggered communication, hierarchical cluster coordination, and self-organized topology adaptation for very large multi-AUV systems.

Author Contributions: Methodology, C.W. and X.L.; writing, review and editing, C.W., P.Y., X.L., J.W. and Y.W.; funding acquisition, X.L. All authors have read and agreed to the published version of the manuscript.

Funding: This work is supported by the open funding of Key Laboratory of System Control and Information Processing, Ministry of Education, Shanghai, 200240, under grant Scip20240109.

Data Availability Statement: Data are all contained within the article.

Conflicts of Interest: The authors declare no conflicts of interest.

References

1. Zhang, B.; Ji, D.; Liu, S.; Zhu, X.; Xu, W. Autonomous underwater vehicle navigation: A review. *Ocean Eng.* **2023**, *273*, 113861. [CrossRef]
2. Yang, Y.; Xiao, Y.; Li, T. A survey of autonomous underwater vehicle formation: Performance, formation control, and communication capability. *IEEE Commun. Surv. Tutor.* **2021**, *23*, 815–841. [CrossRef]
3. González-García, J.; Gómez-Espinosa, A.; Cuan-Urquizo, E.; García-Valdovinos, L.G.; Salgado-Jiménez, T.; Escobedo Cabello, J.A. Autonomous underwater vehicles: Localization, navigation, and communication for collaborative missions. *Appl. Sci.* **2020**, *10*, 1256. [CrossRef]
4. Wen, J.; Yang, J.; Wang, T. Path planning for autonomous underwater vehicles under the influence of ocean currents based on a fusion heuristic algorithm. *IEEE Trans. Veh. Technol.* **2021**, *70*, 8529–8544. [CrossRef]
5. Wen, J.; Wang, A.; Zhu, J.; Xia, F.; Peng, Z.; Zhang, W. Adaptive energy-efficient reinforcement learning for auv 3d motion planning in complex underwater environments. *Ocean Eng.* **2024**, *312*, 119111. [CrossRef]
6. Pi, R.; Cieślak, P.; Ridao, P.; Sanz, P.J. Twinbot: Autonomous underwater cooperative transportation. *IEEE Access* **2021**, *9*, 37668–37684. [CrossRef]
7. Yan, Z.; Zhang, C.; Tian, W.; Cai, S.; Zhao, L. Distributed observer-based formation trajectory tracking method of leader-following multi-auv system. *Ocean Eng.* **2022**, *260*, 112019. [CrossRef]
8. Yan, T.; Xu, Z.; Yang, S.X. Consensus formation tracking for multiple auv systems using distributed bioinspired sliding mode control. *IEEE Trans. Intell. Veh.* **2023**, *8*, 1081–1092. [CrossRef]
9. Shou, Y.; Xu, B.; Zhang, A.; Mei, T. Virtual guidance-based coordinated tracking control of multi-autonomous underwater vehicles using composite neural learning. *IEEE Trans. Neural Netw. Learn. Syst.* **2021**, *32*, 5565–5574. [CrossRef]
10. Shen, C.; Shi, Y. Distributed implementation of nonlinear model predictive control for auv trajectory tracking. *Automatica* **2020**, *115*, 108863. [CrossRef]
11. Liang, X.; Qu, X.; Hou, Y.; Li, Y.; Zhang, R. Distributed coordinated tracking control of multiple unmanned surface vehicles under complex marine environments. *Ocean Eng.* **2020**, *205*, 107328. [CrossRef]
12. Hayakawa, T.; Ishii, H.; Tsumura, K. Adaptive quantized control for linear uncertain discrete-time systems. In Proceedings of the 2005, American Control Conference, Portland, OR, USA, 8–10 June 2005; Volume 7, pp. 4784–4789.

13. Aslmostafa, E.; Ghaemi, S.; Badamchizadeh, M.A.; Ghiasi, A.R. Adaptive backstepping quantized control for a class of unknown nonlinear systems. *ISA Trans.* **2022**, *125*, 146–155. [CrossRef]
14. Liu, T.; Jiang, Z.-P. Event-triggered control of nonlinear systems with state quantization. *IEEE Trans. Autom. Control* **2019**, *64*, 797–803. [CrossRef]
15. Wu, J.; Sun, W.; Su, S.-F.; Xia, J. Neural-based adaptive control for nonlinear systems with quantized input and the output constraint. *Appl. Math. Comput.* **2022**, *413*, 126637. [CrossRef]
16. Zhang, Z.; Wen, C.; Xing, L.; Song, Y. Adaptive output feedback control of nonlinear systems with mismatched uncertainties under input/output quantization. *IEEE Trans. Autom. Control* **2022**, *67*, 4801–4808. [CrossRef]
17. Fossen, T.I. *Guidance and Control of Ocean Vehicles*; John Wiley & Sons: Hoboken, NJ, USA, 1994.
18. Sagatun, S.; Fossen, T. Lagrangian formulation of underwater vehicles' dynamics. In Proceedings of the Conference Proceedings 1991 IEEE International Conference on Systems, Man, and Cybernetics, Charlottesville, VA, USA, 13–16 October 1991; Volume 2, pp. 1029–1034.
19. Ceragioli, F.; De Persis, C.; Frasca, P. Discontinuities and hysteresis in quantized average consensus. *Automatica* **2011**, *47*, 1916–1928. [CrossRef]
20. Li, X.; Wen, C.; Fang, X.; Wang, J. Adaptive bearing-only formation tracking control for nonholonomic multiagent systems. *IEEE Trans. Cybern.* **2022**, *52*, 7552–7562. [CrossRef]
21. Du, P.; Yang, W.; Chen, Y.; Huang, S. Improved indirect adaptive line-of-sight guidance law for path following of under-actuated auv subject to big ocean currents. *Ocean Eng.* **2023**, *281*, 114729. [CrossRef]
22. Zhang, W.; Zeng, J.; Yan, Z.; Wei, S.; Tian, W. Leader-following consensus of discrete-time multi-auv recovery system with time-varying delay. *Ocean Eng.* **2021**, *219*, 108258. [CrossRef]
23. Yan, Z.; Gong, P.; Zhang, W.; Wu, W. Model predictive control of autonomous underwater vehicles for trajectory tracking with external disturbances. *Ocean Eng.* **2020**, *217*, 107884. [CrossRef]
24. Miao, J.; Wang, Y.; Deng, K.; Sun, X.; Liu, W.; Guo, Z. Peclos path-following control of underactuated auv with multiple disturbances and input constraints. *Ocean Eng.* **2023**, *284*, 115236. [CrossRef]
25. Touzout, W.; Benmoussa, Y.; Benazzouz, D.; Moreac, E.; Diguet, J.-P. Unmanned surface vehicle energy consumption modelling under various realistic disturbances integrated into simulation environment. *Ocean Eng.* **2021**, *222*, 108560. [CrossRef]